Continuous Aperture Phased MIMO: Basic Theory and Applications

Akbar Sayeed
Elect. & Comp. Engineering
University of Wisconsin
Madison, WI 53706
Email: akbar@engr.wisc.edu

Nader Behdad
Elect. & Comp. Engineering
University of Wisconsin
Madison, WI 53706
Email: behdad@engr.wisc.edu

Abstract—Given the proliferation of wireless communication devices, the need for increased power and bandwidth efficiency in emerging technologies is getting ever more pronounced. Two technological trends offer new opportunities for addressing these challenges: mm-wave systems (60-100GHz) that afford large bandwidths, and multi-antenna (MIMO) transceivers that exploit the spatial dimension. In particular, there has been significant recent interest in mm-wave communication systems for high-rate (1-100 Gb/s) communication over line-of-sight (LoS) channels. Two competing designs dominate the state-of-the-art: i) traditional systems that employ continuous aperture "dish" antennas and offer high power efficiency but no spatial multiplexing gain, and ii) MIMO systems that use discrete antenna arrays for a higher multiplexing gain but suffer from power efficiency. In this paper, we propose a new communication architecture – continuous aperture phased MIMO – that combines the advantages of both designs and promises very significant capacity gains, and commensurate gains in power and bandwidth efficiency, compared to the state-of-the-art. CAP-MIMO is based on a hybrid analog-digital transceiver architecture that employs a novel antenna array structure – a high-resolution discrete lens array – to enable a continuous aperture phased-MIMO operation. We present the basic theory behind CAP-MIMO and the potential capacity/power gains afforded by it. We also highlight potential applications of CAP-MIMO in mm-wave communications.

I. INTRODUCTION

The proliferation of data hungry wireless applications is driving the demand for higher power and bandwidth efficiency in emerging wireless transceivers. Two recent technological trends offer synergistic opportunities for meeting the increasing demands on wireless capacity: i) MIMO systems that exploit multi-antenna arrays for simultaneously multiplexing multiple data streams, and ii) millimeter-wave communication systems, operating in the 60-100GHz band, that provide larger bandwidths. A key advantage of mm-wave systems is that they offer high-dimensional MIMO operation with relatively compact arrays. In particular, there has been significant recent interest in mm-wave communication systems for high-rate (1-100 Gb/s) communication over line-of-sight (LoS) channels. Two competing designs dominate the state-of-the-art: i) traditional systems[1], which we refer to as DISH systems, that employ continuous aperture "dish" antennas and offer high

---

[1]See, e.g., the commercial technology available from Bridgewave Communications; http://www.bridgewave.com

power efficiency but no spatial multiplexing gain, and ii) MIMO systems that use discrete antenna arrays for a higher multiplexing gain but suffer from power efficiency; see, e.g., [1], [2], [3].

This paper develops the basic theory of a new MIMO transceiver architecture – continuous aperture phased (CAP) MIMO – that combines the elements of MIMO, continuous aperture antennas, and phased arrays for dramatically enhanced performance. CAP-MIMO is based on a *hybrid analog-digital transceiver architecture* that employs a novel antenna array structure – *a high-resolution discrete lens array (DLA)* [4] – to enable a *quasi-continuous aperture* phased-MIMO operation. The DLA-based analog-digital interface also offers a low-complexity/low-cost alternative to *high-dimensional* phased arrays that employ digital beamforming for communication but are too complex and/or expensive to build at this time. In particular, in the context of gigabit LoS communication links, the CAP-MIMO system combines the attractive features of conventional state-of-the-art designs – the power gain of DISH systems and multiplexing gain of MIMO systems – to deliver very significant capacity gains and commensurate gains in power/bandwidth efficiency. Furthermore, the hybrid analog-digital architecture enables precise control of spatial beams for link optimization and point-to-multipoint operation that is not possible with existing designs.

In a high-resolution DLA, a microwave lens with an appropriately designed *quasi-continuous phase profile* serves as the radiating aperture that is excited by feed elements on an associated focal surface [4]. In CAP-MIMO, appropriately digitally processed data streams excite the feed elements on the focal surface and signal propagation from the focal arc to the aperture affects an analog spatial Fourier transform.

The basic mathematical framework for CAP-MIMO developed in this paper relies on a critically sampled discrete representation of continuous aperture antennas or radiating surfaces. The number of critical samples, n, represents the maximum number of *analog spatial modes* that are excitable on the aperture. The resulting sampled system can be conceptualized in two complementary but equivalent ways: i) as an $n \times n$ MIMO system with n-element antenna arrays at the transmitter and the receiver, or ii) as two coupled n-element phased uniform linear arrays (ULAs). We leverage the

connection between MIMO systems and phased ULAs from a communication perspective that was first established in [5] and further developed in [6], [7].

The CAP-MIMO framework is applicable to a very broad class of communication links: short-range versus long-range, LoS versus multipath propagation, point-to-point versus network links. However, our focus is on high-frequency (mm-wave), high-rate (1-1000 Gbps) LoS links, which could either be short-range (as in high-rate indoor applications, e.g. HDTV) or long-range (as in wireless backhaul). In such applications, out of the n possible analog modes, only $p \ll n$ *digital modes* couple the transmitter and the receiver and can be used for simultaneously transmitting p data streams. The CAP-MIMO theory enables us to characterize the capacity for any such LoS link and the DLA-based analog-digital architecture enables us to approach the link capacity in practice with a significantly lower complexity compared to traditional architectures based on phased arrays that employ digital beamforming.

In the next section, we present an overview of the CAP-MIMO system for LoS links with one-dimensional (1D) linear apertures and highlight its advantages over the two state-of-the-art designs: i) conventional DISH systems, and ii) conventional MIMO systems. The basic CAP-MIMO theory for 1D apertures is developed in Sections III-V, extension to 2D apertures is discussed in Sec. VI, representative numerical capacity comparisons are provided in Sec. VII, and details of the DLA-based realization of CAP-MIMO transceivers is discussed in Sec. VIII.

II. OVERVIEW OF CAP-MIMO

Fig. 1 depicts a 1D LoS link in which the transmitter and receiver antennas have a linear aperture of length A and are separated by a distance R. Throughout, we assume that $A \ll R$. Let $\lambda_c = c/f_c$ denote the wavelength of operation, where c is the speed of light and f_c is the carrier frequency. For $f_c \in [60, 100]$GHz, $\lambda_c \in [3, 5]$mm.
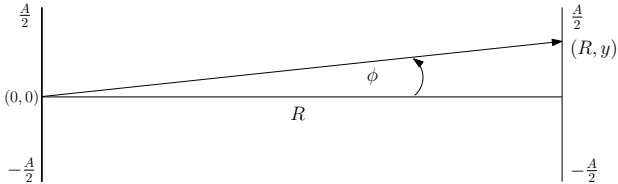
Fig. 1.   The LoS channel.

For a given LoS link characterized by the physical parameters (A, R, λ_c), as in Fig. 1, the CAP-MIMO framework addresses the following fundamental question: **What is the link capacity at any operating signal-to-noise ratio** (SNR)**?** The CAP-MIMO theory is aimed at characterizing this fundamental limit and the DLA-based realization of the CAP-MIMO system is aimed at approaching this limit in practice. As elaborated in this paper, the DISH and MIMO designs are sub-optimum special cases of the CAP-MIMO framework.

Sec. II-A introduces the concept of analog versus digital modes that play a key role in the CAP-MIMO framework.

Sec. II-B introduces the DLA-based hybrid analog-digital architecture of a CAP-MIMO system for efficiently accessing the information carrying digital modes via *analog spatial beamforming*. The complexity of the analog-digital interface of a DLA-based CAP-MIMO system is compared to conventional approaches based on phased-arrays that use *digital beamforming*. Approximate closed-form expressions for capacity are presented in Sec. II-C. Sec. II-D introduces the concept of beamwidth agility for realizing different configurations of a CAP-MIMO system that afford robustness in mobile links.

A. Analog versus Digital Spatial Modes

From a communication perspective, the continuous aperture antennas at the transmitter and the receiver can be equivalently represented by critically sampled (virtual) n-dimensional ULAs with antenna spacing $d = \lambda_c/2$, where $n \approx 2A/\lambda_c$ is a fundamental quantity associated with a linear aperture antenna (electrical length). In other words, the analog spatial signals transmitted or received by the antennas belong to an n-dimensional signal space. We term n as the *maximum number of independent* **analog (spatial) modes** *supported by the antennas*. These n spatial modes can be associated with n orthogonal spatial beams that cover the entire (one-sided) spatial horizon ($-\pi/2 \leq \phi \leq \pi/2$ in Fig. 1) as illustrated in Fig. 2(a). However, due to the finite antenna aperture A, and large distance $R \gg A$ between the transmitter and the receiver, only a small number of modes/beams, $p_{max} \ll n$, couple from the transmitter to the receiver, and vice versa, as illustrated in Fig. 2(b). We term p_{max} as the *maximum number of independent* **digital (spatial) modes** *supported by the LoS link*. The number of digital modes, p_{max}, is a fundamental
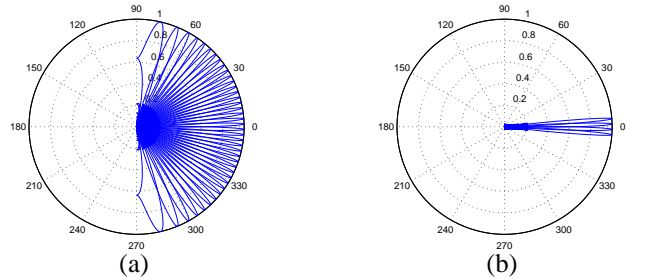
Fig. 2.   CAP-MIMO beampatterns: $n = 40$, $p_{max} = 4$. (a) The $n = 40$ orthogonal beams covering the entire spatial horizon. (b) The $p_{max} = 4$ orthogonal beams that couple the finite aperture antennas.

quantity related to the LoS *link* and can be calculated as $p_{max} \approx A^2/(R\lambda_c)$. In other words, the information bearing signals in the LoS link lie in a p_{max}-dimensional subspace of the n-dimensional signal space associated with the antennas.

B. DLA-based Hybrid Analog-Digital Architecture

Fig. 3 shows a (baseband) schematic of a DLA-based hybrid analog-digital architecture for realizing a CAP-MIMO system. At the transmitter the architecture enables direct access to p digital modes, $1 \leq p \leq p_{max}$, denoted by the input signals $x_e(i), i = 1, \cdots, p$. Any space-time coding technique can be used for encoding information into the p digital inputs
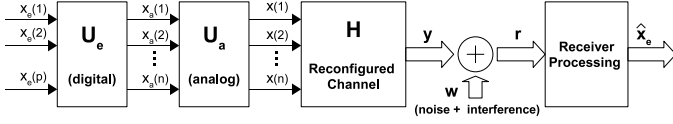
Fig. 3. The hybrid analog-digital architecture of a CAP-MIMO system.

$\{x_e(i)\}$. These digital signals are then mapped into n feed signals, $x_a(i), i = 1, \cdots, n$, on the focal surface of the DLA, via the $n \times p$ digital transform $\mathbf{U}_e$. Different values of p represent the different CAP-MIMO configurations (See Sec. II-C and Sec. II-D). For $p = p_{max}$, $\mathbf{U}_e$ reduces to the identity transform. For $p < p_{max}$, $\mathbf{U}_e$ effectively maps the digital signals to the focal arc so that p data streams are mapped onto p beams with wider beamwidths (see Sec. VIII).

The analog transform $\mathbf{U}_a$ represents the *analog spatial transform* between the focal surface and the continuous radiating aperture of the DLA. This continuous Fourier transform is affected by the wave propagation between the focal surface and the aperture of the DLA. However, this continuous Fourier transform can be accurately approximately by an $n \times n$ discrete Fourier transform (DFT) matrix $\mathbf{U}_a$ (see (14)) corresponding to critical sampling of the aperture and the focal arc (surface in 2D). The analog signals on the DLA aperture are represented by their critically sampled version $x(i), i = 1, \cdots, n$ in Fig. 3.

The DLA-based CAP-MIMO transceiver architecture provides the lowest-complexity analog-digital interface for accessing the p_{max} digital modes in a LoS link. To see this, it is instructive to compare the CAP-MIMO transmitter with a comparable transmitter based on an n-element phased array. In a phased-array, the continuous transmitter aperture in Fig. 1 is replaced with an n-element phased array, where each element is associated with its own RF chain, including an D/A converter and an up-converter. In a phased-array, the p_{max} digital modes can be accessed via *digital beamforming* - each digital mode/beam is associated with an n-dimensional phase profile across the entire n-element phased array. As a result, all n elements of the phased array are involved in encoding the symbol into a corresponding spatial beam via digital beamforming. Thus, the D/A interface of a phased array-based system is n-dimensional or has complexity n.

In a DLA-based CAP-MIMO transmitter, the p_{max} digital modes are accessed via *analog beamforming*. While not shown, the D/A conversion, including up-conversion to the passband at f_c, is done at the output of $\mathbf{U}_e$. That is, the D/A interface is between $\mathbf{U}_e$ and $\mathbf{U}_a$ in Fig. 3. As elaborated in Sec. VIII, even though the digital transform $\mathbf{U}_e$ is $n \times p$ for general operation, only on the order of $p_{max} \ll n$ outputs are non-zero or active and as a result a corresponding number of feed elements (represented by $\{x_a(i)\}$ in Fig. 3) are active on the focal surface of the DLA. Thus, the the D/A interface in a DLA-based CAP-MIMO system has a complexity on the order of p_{max}, rather than the order n complexity in a phased-array.

The receiver also uses a DLA-based architecture to map the analog spatial signals on the DLA aperture to signals in beamspace via n sensors appropriately placed on the focal surface. A subset of n signals on the focal surface of the receiver DLA is then down-converted and converted into baseband digital signals via an A/D. (The complexity of this A/D interface is again on the order of $p_{max} \ll n$, rather than n as in a conventional phased-array-based system.) The digital signals are then appropriately processed, using any of a variety of well-known algorithms, to recover an estimate, $\hat{x}_e(i), i = 1, \cdots, p$, of the transmitted digital signals.

C. Capacity Comparison

In this section, we present idealized closed-form expressions that provide accurate approximations for the capacity of the CAP-MIMO, DISH and MIMO systems for a 1D LoS link depicted in Fig. 1. The rationale behind these closed-form approximations is presented in Sec. IV.

1) Conventional MIMO System: Our starting point is the conventional MIMO system that uses a ULA with p_{max} antennas - p_{max} also reflects the maximum multiplexing gain or the maximum number of *digital modes* supported by the system. The required antenna spacing (Rayleigh spacing) to create p_{max} orthogonal spatial modes is given by

$$d_{ray} = \sqrt{\frac{R\lambda_c}{p_{max}}} \tag{1}$$

and the corresponding aperture is given by

$$A = p_{max} d_{ray} \tag{2}$$

Ignoring path loss, and assuming omnidirectional antennas, the capacity of the conventional MIMO system is given by

$$C_{mimo} = p_{max} \log(1 + \rho\sigma_c^2/p_{max}^2) = p_{max} \log(1 + \rho) \tag{3}$$

where ρ denotes the total transmit SNR (signal-to-noise ratio) and $\sigma_c^2 = p_{max}^2$ is the total channel power (captured by p_{max}^2 transmit and receive omnidirectional antenna pairs). If higher gain antennas are used, the capacity expression (3) can be modified by replacing it with a higher effective ρ.

2) Conventional DISH System: For a given aperture, A, defined in (2), the maximum number of *analog modes*, n, is the number of Nyquist samples, spaced by $d = \lambda_c/2$

$$A = nd = n\frac{\lambda_c}{2} \iff n = \frac{2A}{\lambda_c} . \tag{4}$$

resulting in an $n \times n$ (virtual) MIMO system. The DISH system has a higher total channel power $\sigma_c^2 = n^2$ due to the continuous aperture which, in an ideal setting, is equally distributed between the p_{max} digital modes. Since the DISH system transmits a single data stream, its capacity can be accurately approximated as

$$C_{dish} \approx \log\left(1 + \frac{\rho\sigma_c^2}{p_{max}}\right) = \log\left(1 + \frac{\rho n^2}{p_{max}}\right) \tag{5}$$

3) CAP-MIMO System: The CAP-MIMO system combines the attractive features of DISH (high channel power - antenna gain) with those of MIMO (multiplexing gain). Furthermore, CAP-MIMO system has the agility to adapt the number of data streams, p, $1 \leq p \leq p_{max}$. The capacity of the CAP-MIMO system for any p can be accurately approximated as

$$C_{c-mimo}(\rho) \approx p \log \left(1 + \frac{\rho \sigma_c^2}{p p_{max}} \right) = p \log \left(1 + \frac{\rho n^2}{p p_{max}} \right) \tag{6}$$

where $\sigma_c^2 = n^2$ as in the DISH system. We focus on three CAP-MIMO configurations:

- **Multiplexing (MUX) configuration** – $p = p_{max}$ – that yields the highest capacity.
- **Intermediate (INT) configuration** – $p \approx \sqrt{p_{max}}$ – that yields medium capacity.
- **Beamforming (BF) configuration** – $p = 1$ – that yields the lowest capacity, equal to that of the DISH system.

Fig. 4(a) shows the capacities of different systems along with the three CAP-MIMO configurations. The figure corresponds to a short-range ($R = 3m$) link with linear aperture $A = 16$cm operating at $f_c = 80$ GHz with $p_{max} = 4$ and $n = 85$. As evident, between the two conventional systems, MIMO dominates at high SNRs whereas DISH dominates at low SNRs. CAP-MIMO on the other hand, exceeds the performance of both conventional systems over the entire SNR range. Fig. 4(b) compares DISH, MIMO and CAP-MIMO MUX configuration for a long-range ($R = 1$km) 60GHz link with linear aperture $A = 3.35$m, $p_{max} = 4$ and $n = 1342$. The performance gains of CAP-MIMO over DISH and MIMO are even more pronounced in this case.

(a) Short-range link   (b) Long-range link
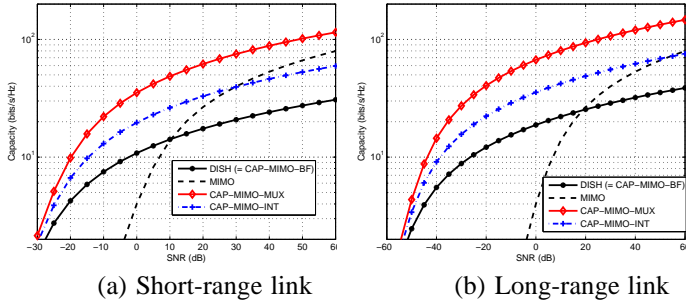
Fig. 4. Capacity comparison for: (a) a short-range ($R = 3$m) 1D link at 80 GHz, (b) long-range ($R = 1$km) 1D link at 60 GHz.

D. CAP-MIMO Configurations: Beam Agility

As noted above, the CAP-MIMO system can achieve a multiplexing gain of $p \in \{1, \cdots, p_{max}\}$ corresponding to different configurations. Lower values of p are advantageous in applications involving mobile links. This is because of the beam agility capability of the CAP-MIMO system: for $p < p_{max}$, by appropriately reconfiguring the digital transform $\mathbf{U}_e$, the p data streams can be encoded into p beams with *wider beamwidths*. The use of wider beamwidths relaxes the channel tracking requirements.

Fig. 5 illustrates the notion of beam agility for a 1D system with $n = 40$ and $p_{max} = 4$. Fig. 5(a) shows the beampatterns

for the MUX configuration for which $p = p_{max} = 4$ and 4 narrow beams couple with the receiver aperture. Fig. 5(b) shows the beampatterns for an INT configuration with $p = 2$. In this case 2 beams are used but the beamwidth is twice the beamwidth in the MUX configuration. Fig. 5(c) shows the beampatterns for the BF configuration with $p = 1$. In this case, a single data stream is encoded into a single beam with the largest beamwidth - 4 times the beamwidth in the MUX configuration. The BF configuration represents an optimized conventional DISH system.
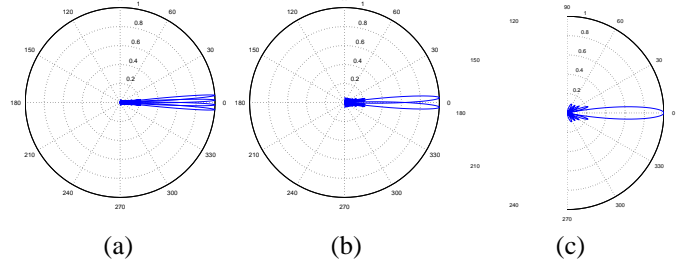
Fig. 5. CAP-MIMO Beampatterns for the three configurations for $n = 40$ and $p_{max} = 4$. (a) MUX $p = 4$. (b) INT $p = 2$, (c) BF $p = 1$.

III. SYSTEM MODEL

In this section, we develop a common framework for developing the basic theory of CAP-MIMO and comparing it with the two conventional designs: continuous-aperture DISH designs, and conventional MIMO designs. Our emphasis is on mm-wave systems in LoS channels. We first develop our framework for one-dimensional (1D) linear arrays and then comment on two-dimensional (2D) arrays in Sec. VI. It is insightful to view the LoS link in Fig. 1 from two perspectives: as a sampled MIMO system and as two coupled phased arrays. This connection between MIMO systems and phased arrays was first established in [5].

A. The LoS Channel: MIMO meets Phased Arrays

Fig. 1 depicts the LoS channel in the 1D setting. The transmitter and receiver consist of a continuous linear aperture of length A and are separated by a distance $R \gg A$. The center of the receiver array serves as the coordinate reference: the receiver array is described by the set of points $\{(x, y) : x = 0, -A/2 \leq y \leq A/2\}$ and the transmitter array is described by $\{(x, y) : x = R, -A/2 \leq y \leq A/2\}$. While the LoS link can be analyzed using a continuous representation [6], in this paper we focus on a critically sampled system description, with spacing $d = \lambda_c/2$, that results in no loss of information and provides a convenient finite-dimensional system description for developing our framework [5].

For a given spacing d, the point-to-point LoS link in Fig. 1 can be described by an $n \times n$ MIMO system

$$\mathbf{r} = \mathbf{H}\mathbf{x} + \mathbf{w} \tag{7}$$

where $\mathbf{x} \in \mathcal{C}^n$ is the transmitted signal, $\mathbf{r} \in \mathcal{C}^n$ is the received signal, $\mathbf{w} \sim \mathcal{CN}(\mathbf{0}, \mathbf{I})$ is the AWGN noise vector, $\mathbf{H}$ is the

$n \times n$ channel matrix, and the system dimension is given by

$$n = \left\lfloor \frac{A}{d} \right\rfloor . \tag{8}$$

For critical spacing $d = \lambda_c/2$, $n \approx 2A/\lambda_c$ which represents the maximum number of independent spatial (analog) modes excitable on the array apertures.

The fundamental performance limits of the LoS link are governed by (the eigenvalues of) the channel matrix $\mathbf{H}$. In this paper, we will consider beamspace representation of $\mathbf{H}$ [5]. Furthermore, we will be dealing with discrete representations of signals both in the spatial and beamspace domains. We use the following convention for the set of (symmetric) indices for describing a discrete signal of length n

$$\mathcal{I}(n) = \{i - (n-1)/2 : i = 0, \cdots, n-1\} . \tag{9}$$

It is convenient to use the *spatial frequency* (or normalized angle) θ that is related to ϕ as [5]

$$\theta = \frac{d}{\lambda_c} \sin(\phi) . \tag{10}$$

The beamspace channel representation is based on n-dimensional array response/steering (column) vectors, $\mathbf{a}_n(\theta)$, that represent a plane wave associated with a point source in the direction θ. The elements of $\mathbf{a}_n(\theta)$ are given by

$$a_{n,i}(\theta) = e^{-j2\pi\theta i} , \quad i \in \mathcal{I}(n) \tag{11}$$

Note that $\mathbf{a}(\theta)$ are periodic in θ with period 1 and

$$\mathbf{a}_n^H(\theta')\mathbf{a}_n(\theta) = \sum_{i \in \mathcal{I}(n)} a_{n,i}(\theta)a_{n,i}^*(\theta') = \sum_{i \in \mathcal{I}(n)} e^{-j2\pi(\theta-\theta')n}$$
$$= \frac{\sin(\pi n(\theta - \theta'))}{\sin(\pi(\theta - \theta'))} \triangleq f_n(\theta - \theta') \tag{12}$$

where $f_n(\theta)$ is the Dirichlet sinc function, with a maximum of n at $\theta = 0$, and zeros at multiples of $\Delta\theta_o$ where

$$\Delta\theta_o = \frac{1}{n} \approx \frac{d}{A} \iff \Delta\phi_o \approx \frac{\lambda_c}{d}\Delta\theta_o = \frac{\lambda_c}{A} \tag{13}$$

which is a measure of the *spatial resolution* or the *width of a beam* associated with an n-element phased array.

The n-dimensional signal spaces, associated with the transmitter and receiver in an $n \times n$ MIMO system, can be described in terms of the n orthogonal spatial beams represented by appropriately chosen steering/response vectors $\mathbf{a}_n(\theta)$ defined in (11). For an n-element ULA, with $n = A/d$, an orthogonal basis for the $\mathcal{C}^n$ can be generated by uniformly sampling $\theta \in [-1/2, 1/2]$ with spacing $\Delta\theta_o$ [5]. That is,

$$\mathbf{U}_n = \frac{1}{\sqrt{n}}[\mathbf{a}_n(\theta_i)]_{i \in \mathcal{I}(n)} , \quad \theta_i = i\Delta\theta_o = \frac{i}{n} = i\frac{d}{A} \tag{14}$$

is an orthogonal (DFT) matrix with $\mathbf{U}_n^H\mathbf{U}_n = \mathbf{U}_n\mathbf{U}_n^H = \mathbf{I}$. For critical spacing, $d = \lambda_c/2$, the orthogonal beams corresponding to the columns of $\mathbf{U}_n$, cover the entire range for physical angles $\phi \in [-\pi/2, \pi/2]$.

For developing the beamspace channel representation we note in Fig. 1 that a point y on the transmitter array represents a plane wave impinging on the receiver array from the direction $\phi \approx \sin(\phi)$ with the corresponding θ given by (10)

$$\sin(\phi) = \frac{y}{\sqrt{R^2 + y^2}} \approx \frac{y}{R} \iff \theta = \frac{dy}{\lambda_c R} \tag{15}$$

Using (15), we get the following correspondence between the sampled points on the transmitter array and the angles subtended at the receiver array

$$y_i = id \iff \theta_i = i\frac{d^2}{R\lambda_c} , \quad i \in \mathcal{I}(n) \tag{16}$$

which for critical sampling $d = \lambda_c/2$ reduces to

$$y_i = i\frac{\lambda_c}{2} \iff \theta_i = i\frac{\lambda_c}{4R} , i \in \mathcal{I}(n). \tag{17}$$

Finally, the n columns of matrix $\mathbf{H}$ are given by $\mathbf{a}(\theta)$ corresponding to the θ_i in (17); that is,

$$\mathbf{H} = [\mathbf{a}_n(\theta_i)]_{i \in \mathcal{I}(n)} , \quad \theta_i = i\Delta\theta_{ch} = i\frac{\lambda_c}{4R} . \tag{18}$$

We define the total channel power as

$$\sigma_c^2 = \text{tr}(\mathbf{H}^H\mathbf{H}) = n^2 . \tag{19}$$

B. Channel Rank: Coupled Orthogonal Beams

For the LoS link in Fig. 1, the link capacity is directly related to the rank of $\mathbf{H}$ which is in turn related to the number of orthogonal beams from the transmitter that lie within the aperture of the receiver array, which we will refer to as the *maximum number of digital modes*, p_{max}. Fig. 2(a) shows the far-field beampatterns corresponding to the n orthogonal beams defined in (14) for $n = 40$ that cover the entire spatial horizon. Of these beams, only $p_{max} = 4$ couple to the receiver array with a limited aperture, as illustrated in Fig. 2(b). The number p_{max} can be calculated as

$$p_{max} = \frac{2\theta_{max}}{\Delta\theta_o} = 2\theta_{max}n = 2\theta_{max}\frac{A}{d} \approx \frac{A^2}{R\lambda_c} \tag{20}$$

where $\theta_{max} = 0.5\sin(\phi_{max})$ denotes the *(normalized) angular spread* subtended by the receiver array at the transmitter; we have used (10) and (15), noting that $\sin(\phi_{max}) \approx \frac{A}{2R}$, where ϕ_{max} denotes the physical (one-sided) angular spread subtended by the receiver array at the transmitter.

We note that p_{max} in (20) is a fundamental link quantity that is independent of the antenna spacing used. For the conventional DISH system and the CAP-MIMO system we use $d = \lambda_c/2$. A conventional MIMO system, on the other hand, uses p_{max} antennas with spacing d_{ray}; plugging $A = p_{max}d$ in (20) leads to the required (Rayleigh) spacing d_{ray} in (1). The maximum number of digital modes, p_{max}, defined in (20) is a baseline indicator of the rank of the channel matrix $\mathbf{H}$. The actual rank depends on the number of dominant eigenvalues of $\mathbf{H}^H\mathbf{H}$ as discussed in Sec. V.

C. CAP-MIMO versus MIMO Beampatterns: Grating Lobes

Fig. 6 illustrates a key difference in the beampatterns of a CAP-MIMO system and a MIMO system. Fig. 6(a) illustrates two of the $p_{max} = 4$ orthogonal beams that couple with the receiver in a CAP-MIMO system with $n = 40$. Fig. 6(b) illustrates the same two beams corresponding to a MIMO system with p_{max} antennas with spacing d_{ray}. As evident, each beam exhibits $n_c = n/p_{max} = 10$ peaks – one of which lies within the receiver aperture while the remaining 9 (grating lobes) do not couple to the receiver.[2] These grating lobes result in overall channel power loss proportional to n_c^2 compared to the CAP-MIMO system. The grating lobes also result in a loss of security and increased interference.
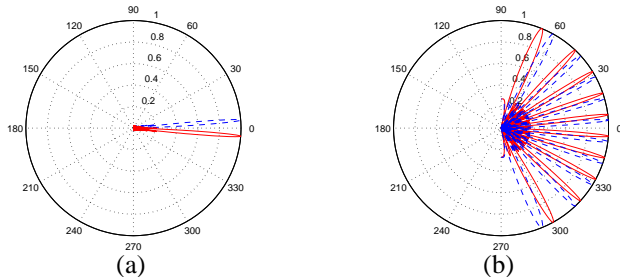
Fig. 6. CAP-MIMO versus MIMO beampatterns: $n = 40$, $p_{max} = 4$. (a) CAP-MIMO beampatterns for two of the p_{max} beams that couple with the receiver. (b) MIMO beampatterns for the same two beams – the grating lobes associated with each beam result in loss of channel power.

IV. IDEALIZED CAPACITY ANALYSIS: ARRAY GAIN, CHANNEL POWER, DIGITAL MODES

We now outline the derivation of idealized capacity expressions in Sec. II-C. Consider a LoS with a given n and p_{max}. It is well-known in antenna theory that the array/beamforming gain of a linear array of aperture A is proportional to $n = A/(\lambda_c/2)$. This gain is achieved at the both the transmitter and receiver ends. However, for a given p_{max}, while the entire array aperture is exploited at the transmitter side for each beam, only a fraction $1/p_{max}$ of the aperture is associated with a beam on the receiver side (see Fig. 2). As a result, the total transmit-receiver array/beamforming gain associated with each beam or digital mode is n^2/p_{max}. In the ideal setting, the transmit covariance matrix $\mathbf{H}^H\mathbf{H}$ has p_{max} non-zero eigenvalues, each of size n^2/p_{max}, corresponding to the total channel power of $\sigma_c^2 = n^2$. Distributing the total transmit SNR, ρ, equally over these p_{max} eigenmodes gives the CAP-MIMO capacity formula in (6) for $p = p_{max}$.

The CAP-MIMO capacity formula applies for all $p = 1, 2, \cdots, p_{max}$. In particular, for $p = 1$, the CAP-MIMO capacity gives the maximum capacity for the (optimized) DISH system in which the link characteristics are adjusted so that $p_{max} = 1$. If $p_{max} > 1$, then the capacity of a DISH system can be bounded as

$$\log\left(1 + \frac{\rho n^2}{p_{max}}\right) \leq C_{dish} = \log(1 + \rho\lambda_{max}) \leq \log(1 + \rho n^2) \tag{21}$$

[2] We note that $d_{ray} \approx n_g\lambda_c/2$.

where λ_{max} is the largest eigenvalue of $\mathbf{H}^H\mathbf{H}$ and satisfies $n^2/p_{max} = \sigma_c^2/p_{max} \leq \lambda_{max} \leq \sigma_c^2 = n^2$. The capacity expression in (5) corresponds to the lower bound in (21).

The MIMO system uses p_{max} antennas with spacing d_{ray} given in (1). As a result the channel power is p_{max}^2 which, along with total transmit power, is equally distributed within the p_{max} eigenmodes resulting in the capacity expression (3).

V. EXACT CAPACITY ANALYSIS

We now outline exact capacity analysis of the CAP-MIMO system that refines the approximate/idealized capacity expressions in Sec. II-C. The capacity expression (3) for the MIMO system is exact. We consider a static point-to-point LoS channel for which the critically sampled channel matrix $\mathbf{H}$ in (18) is deterministic and we assume that it is completely known at the transmitter and the receiver. In this case, it is well-known that the capacity-achieving input is Gaussian and is characterized by the eigenvalue decomposition of the $n \times n$ transmit covariance matrix [8], [9]

$$\boldsymbol{\Sigma}_T = \mathbf{H}^H\mathbf{H} = \mathbf{V}\boldsymbol{\Lambda}\mathbf{V}^H \tag{22}$$

where $\mathbf{V}$ is the matrix of eigenvectors and $\boldsymbol{\Lambda} = \text{diag}(\lambda_1, \cdots, \lambda_n)$ is the diagonal matrix of eigenvalues with $\sum_i \lambda_i = \sigma_c^2 = n^2$. In particular, the capacity-achieving input vector $\mathbf{x}$ in (7) is characterized as $\mathcal{CN}(\mathbf{0}, \mathbf{V}\boldsymbol{\Lambda}_s\mathbf{V}^H)$ where $\boldsymbol{\Lambda}_s = \text{diag}(\rho_1, \cdots, \rho_n)$ is the diagonal matrix of eigenvalues of the input covariance matrix $E[\mathbf{xx}^H]$ with $\text{tr}(\boldsymbol{\Lambda}_s) = \sum_i \rho_i = \rho$. The capacity of the critically sampled LoS link is then given by

$$C(\rho) = \max_{\boldsymbol{\Lambda}_s:\text{tr}(\boldsymbol{\Lambda}_s)=\rho} \log|\mathbf{I} + \boldsymbol{\Lambda}\boldsymbol{\Lambda}_s| = \max_{\rho_i:\sum_i \rho_i=\rho} \sum_{i=1}^{n} \log(1+\lambda_i\rho_i) \tag{23}$$

As discussed earlier, out of the n possible communication modes, we expect only p_{max} modes/beams to couple to the receiver array. However, the value of p_{max} in (20) provides only an approximate baseline value for the actual channel rank for a given (A, R, λ_c). In numerical results, we replace p_{max} with the effective channel rank, p_{eff}, which we estimate as the number of dominant eigenvalues of $\boldsymbol{\Sigma}_T$ - eigenvalues that are above a certain fraction $\gamma \in (0, 1)$ of λ_{max}:

$$p_{eff} = |\{i : \lambda_i \geq \gamma\lambda_{max}\}| \tag{24}$$

and approximate the system capacity as

$$\begin{aligned}
C(\rho) &\approx \max_{\rho_i:\sum_i^{p_{eff}} \rho_i=\rho} \sum_{i=1}^{p_{eff}} \log(1 + \lambda_i\rho_i) \\
&\geq \sum_{i=1}^{p_{eff}} \log\left(1 + \lambda_i\frac{\rho}{p_{eff}}\right)
\end{aligned} \tag{25}$$

where the last inequality corresponds to equal power allocation to all the p_{eff} modes. As we discuss in our numerical results, the effective channel rank, p_{eff}, is somewhere in the range

$$p_{eff} \in [\lceil p_{max} \rceil, \lceil p_{max} + 1 \rceil]. \tag{26}$$
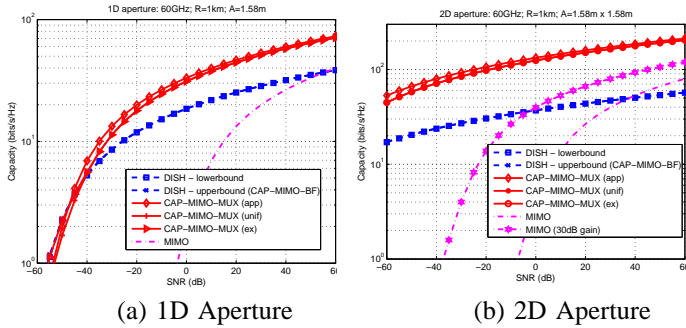
Fig. 7. Capacity versus SNR comparison between the CAP-MIMO, DISH and MIMO systems for a long-range link; $R = 1$km. (a) 1D linear aperture with $A = 1.58$m. (b) 2D square aperture.

Fig. 8. Capacity versus SNR comparison between the CAP-MIMO, DISH and MIMO systems for a short-range link; $R = 3$m. (a) 1D linear aperture with $A = 7.5$cm. (b) 2D square aperture.

VI. TWO-DIMENSIONAL ARRAYS

We now outline the system model for 2D square apertures. Consider a LoS link in which both the transmitter and the receiver antennas, separated by a distance of R meters, consist of square apertures of dimension $A \times A$ m^2. The maximum number of analog and digital modes are simply the squares of the linear counterparts: $n_{2d} = n^2$, $p_{max,2d} = p_{max}^2$. The resulting MIMO system is characterized by the $n_{2d} \times n_{2d}$ matrix $\mathbf{H}_{2d}$ that can be shown to be related to the 1D channel matrix $\mathbf{H}$ in (18) via $\mathbf{H}_{2d} = \mathbf{H} \otimes \mathbf{H}$, where $\otimes$ denotes the kronecker product [10]. The eigenvalue decomposition of the transmit covariance matrix is similarly related to its 1D counterpart in (22): $\mathbf{\Sigma}_{T,2d} = \mathbf{H}_{2d}^H \mathbf{H}_{2d} = \mathbf{V}_{2d} \mathbf{\Lambda}_{2d} \mathbf{V}_{2d}^H$ and $\mathbf{V}_{2d} = \mathbf{V} \otimes \mathbf{V}$, $\mathbf{\Lambda}_{2d} = \mathbf{\Lambda} \otimes \mathbf{\Lambda}$. The channel power is also the square of the 1D channel power: $\sigma_{c,2d}^2 = n_{2d}^2 = n^4 = \sigma_c^4$. With these correspondences, the idealized capacity expressions in Sec. II and the exact capacity analysis in Sec. V can be used.

VII. NUMERICAL RESULTS

We now present numerical results to illustrate the capacity/SNR advantage of the CAP-MIMO system over conventional DISH and MIMO systems. Fig. 7 compares the three systems for a long range link, $R = 1$km, at $f_c = 60$GHz. Fig. 7(a) compares linear apertures with $A = d_{ray} = 1.58$m corresponding to $n = 632$ and $p_{max} = 2$. Fig. 7(b) presents the comparison for a corresponding 2D array with a square aperture of $1.58 \times 1.58m^2$, with $n_{2d} = n^2 = 399424$ and $p_{max,2d} = p_{max}^2 = 4$. Two dominant eigenvalues are used in the 1D system ($\gamma = .01$) and 4 in the 2D system ($\gamma = .001$). In the 2D case, we also include the capacity of a MIMO system with 30dB-gain directional antennas. Fig. 8 compares the three systems for a short-range (indoor) link, $R = 3$m, at $f_c = 80$GHz. Fig. 8(a) compares linear apertures with $A = d_{ray} = 7.5$cm corresponding to $n = 40$ and $p_{max} = 2$. Fig. 8(b) presents the comparison for a corresponding 2D array with a square aperture of $7.5 \times 7.5cm^2$, with $n_{2d} = 1600$ and $p_{max,2d} = 4$. Two dominant eigenvalues are used in the 1D system ($\gamma = .01$) and 4 in the 2D system ($\gamma = .001$).

Interestingly, in both above examples, the condition numbers, $\chi = \lambda_{max}/\lambda_{min}$, for the subset of eigenvalues used, are $\chi_{1d} = 14$ and $\chi_{2d} = 216$. Even though the channel can support up to $p_{eff} = 2$ modes for linear arrays, $p_{max} = 0.5$,
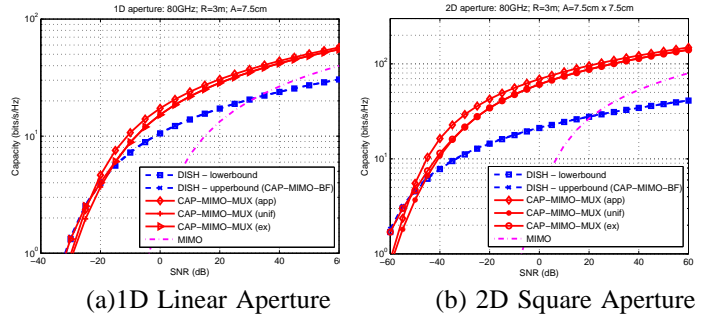
as calculated according to (20), emphasizing the fact that (20) is a baseline estimate (see the range for p_{eff} in (26)). The numerical results correspond to first determining d_{ray} and then using the minimum aperture $A = (p_{max} - 1)d_{ray}$.

As evident from the above results, there is close agreement between the exact and approximate capacity estimates. Furthermore, the CAP-MIMO system exhibits very significant SNR gains over the MIMO and DISH systems at high spectral efficiencies (> 20 bits/s/Hz); about 20dB for linear apertures and more than 40dB for square apertures.

VIII. DETAILS OF THE CAP-MIMO TRANSCEIVER

Fig. 3 shows a schematic of a DLA-based realization of a CAP-MIMO system. In this section, we provide details on the CAP-MIMO transmitter for 1D apertures.

The analog transform $\mathbf{U}_a$ represents the analog spatial Fourier transform between the focal surface and the continuous aperture of the DLA, that is affected by the wave propagation between the focal arc and the aperture. However, we can accurately approximate this continuous Fourier transform by an $n \times n$ discrete Fourier transform (DFT) matrix corresponding to critical sampling of the aperture and the focal arc:

$$\mathbf{U}_a(\ell, m) = \frac{1}{\sqrt{n}} e^{-j\frac{2\pi\ell m}{n}} \quad , \quad \ell \in \mathcal{I}(n) \ , \ m \in \mathcal{I}(n) \quad (27)$$

where ℓ represents samples on the aperture (spatial domain) and m represents samples on the focal arc (beamspace).

The CAP-MIMO architecture is based on a high-resolution DLA to approximate a continuous-aperture phased-MIMO operation. Fig. 9 provides a comparison between a double convex
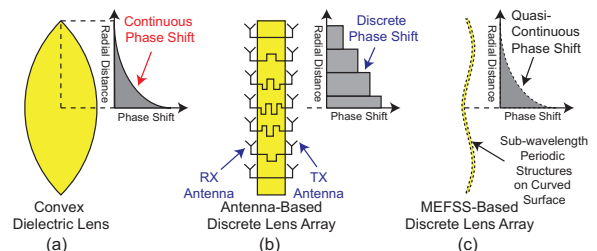
Fig. 9. Comparison between a dielectric lens (a), a traditional microwave lens composed of arrays of receiving and transmitting antennas (b), and the proposed conformal metamaterial-based microwave DLA composed of sub-wavelength periodic structures (c).

dielectric lens, a conventional microwave lens composed of arrays of receiving and transmitting antennas connected through transmission lines with variables lengths (see, e.g., [11], [12], [13], [14], [15], and a high-resolution DLA that we plan to use in this work [4]. The high-resolution DLA is composed of a number of spatial phase shifting elements, or pixels, distributed on a flexible membrane. The local transfer function of the pixels can be tailored to convert the electric field distribution of an incident electromagnetic (EM) wave at the lens' input aperture to a desired electric field distribution at the output aperture. These high-resolution DLAs have several unique advantages over conventional antenna-based microwave lenses, including: 1) The pixels are ultra-thin and their dimensions can be extremely small, e.g. $0.05\lambda_c \times 0.05\lambda_c$ as opposed to $\lambda_c/2 \times \lambda_c/2$ in conventional DLAs [4]. This offers a higher resolution in designing the aperture phase profile; 2) Due to the small pixel sizes, high-resolution DLAs have large field of views of $\pm 70°$; and 3) Unlike conventional microwave lenses, high-resolution DLAs can operate over extremely wide bandwidths with fractional bandwidths exceeding 50%.

The $n \times p$ digital transform $\mathbf{U}_e$ represents mapping of the p, $1 \le p \le p_{max}$, digital signals onto the focal arc (surface in 2D), which is represented by n samples. Different values of p represent the different CAP-MIMO configurations. For $p = p_{max}$, $\mathbf{U}_e$ reduces to $p_{max} \times p_{max}$ identity transform; that is, the p_{max} inputs are directly mapped to corresponding p_{max} feeds on the focal arc. For $p < p_{max}$, $\mathbf{U}_e$ effectively maps the independent digital signals to the focal arc so that p data streams are mapped onto p beams with wider beamwidths. Wider beamwidths, in turn, are attained via excitation of part of the aperture. An explicit construction of $\mathbf{U}_e$ is given next.

For a given p define the *oversampling factor* as $n_{os}(p) = p_{max}/p$, $p = 1, \cdots, p_{max}$. The p digital streams are mapped into p beams that are generated by a reduced aperture $A(p) = A/n_{os}$ with $n_a(p) = n/n_{os} = np/p_{max}$ Nyquist samples. The resulting (reduced) beamspace resolution is given by $\Delta\theta(p) = 1/n_a(p) = (1/n)(p_{max}/p) = \Delta\theta_o n_{os}(p)$, where $\Delta\theta_o = 1/n$ is the (highest, finest) spatial resolution afforded by the full aperture. The reduced resolution corresponds to a larger beamwidth for each beam.

The $n \times p$ digital transform $\mathbf{U}_e$ consists of two components: $\mathbf{U}_e = \mathbf{U}_2\mathbf{U}_1$. The $n_a(p) \times p$ transform $\mathbf{U}_1$ represents the beamspace to aperture mapping for the p digital signals corresponding to an aperture with $n_a(p)$ (Nyquist) samples:

$$\mathbf{U}_1(\ell, m) = \frac{1}{\sqrt{n_a(p)}} e^{-j\frac{2\pi\ell m}{n_a(p)}} = \sqrt{\frac{n_{os}}{n}} e^{-j\frac{2\pi\ell m n_{os}}{n}} \quad , \quad (28)$$

where $\ell \in \mathcal{I}(n_a(p))$, $m \in \mathcal{I}(p)$. The $n \times n_a(p)$ matrix $\mathbf{U}_2$ represents an oversampled - by a factor n_{os} - IDFT (inverse DFT) of the $n_a(p)$ dimensional signal at the output of $\mathbf{U}_1$:

$$\mathbf{U}_2(\ell, m) = \frac{1}{\sqrt{n}} e^{j\frac{2\pi\ell m}{n}} \quad , \quad \ell \in \mathcal{I}(n) \quad , \quad m \in \mathcal{I}(n_a(p)) \quad (29)$$

For a given n, p_{max}, and p, the $n \times p$ composite digital

transform, $\mathbf{U}_e$, can be expressed as

$$
\begin{aligned}
\mathbf{U}_e(\ell, m) &= (\mathbf{U}_2\mathbf{U}_1)(\ell, m) = \sum_{i \in \mathcal{I}(n_a(p))} \mathbf{U}_2(\ell, i)\mathbf{U}_1(i, m) \\
&= \frac{1}{\sqrt{n_{os}}}\frac{1}{n_a} \sum_{i \in \mathcal{I}(n_a)} e^{j2\pi(\frac{\ell - mn_{os}}{n_{os}})\frac{i}{n_a}} \\
&= \frac{1}{\sqrt{n_{os}}n_a} f_{n_a}\left(\frac{1}{n_a}\left(\frac{\ell}{n_{os}} - m\right)\right) \quad , \quad (30)
\end{aligned}
$$

where $f_n(\cdot)$ is defined in (12), $\ell \in \mathcal{I}(n)$ represent the samples of the focal arc of DLA and $m \in \mathcal{I}(p)$ represent the index for the digital data streams. Note that for $p = p_{max}$, $\mathbf{U}_e$ reduces to a $p_{max} \times p_{max}$ identity matrix. Even for $p < p_{max}$, only a subset, on the order of p_{max}, of the outputs of $\mathbf{U}_e$ are active, which can be estimated from (30).

The columns of $\mathbf{U}_e$ serve as approximate transmit eigenfunctions. Transmission on exact eigenmodes can be accomplished by including a $p \times p$ preprocessing matrix $\mathbf{U}_{red}$ which is the matrix of eigenvectors of $\mathbf{H}_{red}^H\mathbf{H}_{red}$ where $\mathbf{H}_{red} = \mathbf{H}\mathbf{U}_a\mathbf{U}_e$ is the $n \times p$ reduced dimensional channel matrix. That is, $\mathbf{U}_e \to \mathbf{U}_e\mathbf{U}_{red}$.

IX. Acknowledgement

References

[1] E. Torkildson, B. Ananthasubramaniam, U. Madhow, and M. Rodwell, "Millimeter-wave MIMO: Wireless links at optical speeds," *Proc. Allerton Conference*, Sep. 2006.

[2] C. Sheldon, M. Seo, E. Torkildson, M. Rodwell, and U. Madhow, "Four-channel spatial multiplexing over a millimeter-wave line-of-sight link," *Proc. IEEE MTT-S Int. Microwave Symp.*, June 2009.

[3] F. Bohagen, P. Orten, and G. Oien, "Design of optimal high-rank line-of-sight MIMO channels," *IEEE Tran. Wireless Commun.*, Apr. 2007.

[4] M. A. Al-Joumayly and N. Behdad, "Design of conformal, high-resolution microwave lenses using sub wavelength periodic structures," in *2010 IEEE Antennas and Propagat. Symp.*, 2010.

[5] A. M. Sayeed, "Deconstructing multi-antenna fading channels," *IEEE Trans. Signal Processing*, vol. 50, no. 10, pp. 2563–2579, Oct. 2002.

[6] T. Deckert and A. M. Sayeed, "A Continuous Representation of Multi-Antenna Fading Channels and Implications for Capacity Scaling and Optimum Array Design," *Proc. IEEE Globecom*, 2003.

[7] A. M. Sayeed and V. Raghavan, "Maximizing MIMO Capacity in Sparse Multipath with Reconfigurable Antenna Arrays," *IEEE J. Select. Topics in Signal Processing*, pp. 156–166, June 2007.

[8] I. E. Telatar, "Capacity of Multi-Antenna Gaussian Channels," *Eur. Trans. Telecommun.*, vol. 10, pp. 585–595, Nov. 1999.

[9] V. Veeravalli, Y. Liang, and A. Sayeed, "Correlated MIMO wireless channels: Capacity, optimal signaling and asymptotics," *IEEE Trans. Inform. Th.*, Jun. 2005.

[10] J. W. Brewer, "Kronecker products and matrix calculus in system theory," *IEEE Trans. Circ. and Syst.*, pp. 772–781, Sep. 1978.

[11] W. Shiroma, E. Bryeron, S. Hollung, and Z. Popovic, "A quasi-optical receiver with angle diversity," in *Proc. IEEE Intl. Microwave Symp.*, 1996, pp. 1131–1135.

[12] D. T. McGrath, "Planar three-dimensional constrained lens," *IEEE Trans. Antennas Propagat.*, vol. 34, no. 1, p. 4650, Jan. 1986.

[13] Z. P. S. Hollung and A. Cox, "A bi-directional quasi-optical lens amplifier," *IEEE Trans. Microwave Th. Techn.*, Dec. 1997.

[14] Z. Popovic and A. Mortazawi, "Quasi-optical transmit/receive front end," *IEEE Trans. Microwave Th. Techn.*, pp. 1964–1975, Nov 1998.

[15] A. Abbaspour-Tamijani, K. Sarabandi, and G. M. Rebeiz, "A planar filter-lens array for millimeter-wave applications," in *Proc. IEEE Intl. Antennas Propag.*, vol. 1, 2004, pp. 675–678.